IOPscience iopscience.iop.org

Home Search Collections Journals About Contact us My IOPscience

Influence of F centres on structural and electronic properties of AlN single-walled nanotubes

This article has been downloaded from IOPscience. Please scroll down to see the full text article.

2007 J. Phys.: Condens. Matter 19 395021

(http://iopscience.iop.org/0953-8984/19/39/395021)

View the table of contents for this issue, or go to the journal homepage for more

Download details:
IP Address: 129.252.86.83
The article was downloaded on 29/05/2010 at 06:07

Please note that terms and conditions apply.

IOP PUBLISHING JOURNAL OF PHYSICS: CONDENSED MATTER

J. Phys.: Condens. Matter **19** (2007) 395021 (18pp) doi:10.1088/0953-8984/19/39/395021

Influence of F centres on structural and electronic properties of AlN single-walled nanotubes

Yu F Zhukovskii[1,2,7], **N Pugno**[3], **A I Popov**[1,4], **C Balasubramanian**[5,6] **and S Bellucci**[5]

[1] Institute for Solid State Physics, University of Latvia, Kengaraga 8, Riga LV-1063, Latvia
[2] Materials Research Center, Northwestern University, 2145 Sheridan Road, Evanston, IL 60208, USA
[3] Department of Structural Engineering, Politecnico di Torino, Corso Duca degli Abruzzi 24, 10129 Torino, Italy
[4] Institut Laue-Langevin, 6 rue Jules Horowitz, 38042 Grenoble, France
[5] INFN-Laboratori Nazionali di Frascati, Via Enrico Fermi 40, I-00044 Frascati, Italy
[6] Department of Environmental, Occupational and Social Medicine, University of Rome Tor Vergata, Via Montpellier 1, I-00133 Rome, Italy

E-mail: quantzh@latnet.lv

Received 13 February 2007, in final form 22 March 2007
Published 30 August 2007
Online at stacks.iop.org/JPhysCM/19/395021

Abstract

We analyse the influence of uncharged N vacancies (neutral F centres), created either under conditions of AlN nanotube growth or by its soft irradiation, on the atomic and electronic structure. Periodic one-dimensional (1D) density functional theory (DFT) calculations on models of defective single-walled nanotubes (SW NTs) allow us to analyse how NT chirality and concentration of F centres change their properties compared to the corresponding defect-free nanotubes. We have simulated reconstruction around periodically repeated F centres on 1 nm AlN SW NTs with armchair- and zigzag-type chiralities. To achieve the limit of an isolated vacancy for both chiralities, we have considered different inter-defect distances repeated along the axes of these nanotubes. For $d_{\mathrm{F-F}} \geqslant 20$ Å, the interaction between defects is found to be negligible, since energy dispersion does not exceed 0.02 eV. We also analyse the influence of F centres on the energy cost required to wrap up AlN graphitic nanosheets (NSs) of both chiralities into the corresponding 1 nm thick SW NTs. The electronic properties of defective NS and NTs of both chiralities have been compared with those for defective AlN bulk three-dimensional (3D) structures of wurtzite and zinc-blend. The presence of N vacancies in various aluminium nitride structures (including SW NTs) results in the appearance of defect energy levels in the band gap with the prevailing contribution from 3s and 3p atomic orbitals of the nearest Al atoms. We have found that the larger the concentration of F centres is, the smaller the maximal energy gap between defect levels is, i.e. an increase

[7] Author to whom any correspondence should be addressed.

in defect content in AlN NTs results in their higher conductivity. Our DFT calculations of point defects on SW NTs have been correlated with theoretical prediction for electrical breakdown voltage induced on a defective nanotube upon removing a single bond.

(Some figures in this article are in colour only in the electronic version)

1. Introduction

In recent years III–V semiconductor nanostructures (nanotubes, nanowires, nanoclusters and nanotips) have attracted enhanced scientific interest due to their numerous technological applications in nanoengineering [1–4], such as optoelectronic devices in the ultraviolet (UV) and visible regions [5]. AlN nanotubes (NTs) of a wide range of diameters (up to 80 nm) were recently synthesized either by simply nitriding impregnated Al powder in a tubular furnace [6] or using the method of highly non-equilibrium direct-current arc-plasma-induced melting of aluminium in N–Ar ambient [7]. So far, systematic theoretical studies on defect-free nanotubes of group-III nitrides, which began several years ago, have been limited mainly to single-walled (SW) models, as analysed in our last paper [8]. The first theoretical paper that considers a multi-walled (MW) AlN NT has been just published [5]. Meanwhile, experimental conditions of the nanotube growth [6, 7] unavoidably lead to both chemical and mechanical reasons for the appearance of point defects, such as vacancies, antisites or substitutional impurities [9]. The controlled creation of atomic vacancies on carbon (C) and BN nanotubular structures can be caused by soft irradiation, for example *in situ* under the influence of the energetic electron beam in a transmission electron microscope (TEM) [10–12]. However, still no reference was found in the literature on the application of the analogous method for vacancy formation in AlN NTs; only transformations in the wurtzite-like AlN bulk structure under sub-angström-resolution scanning tunnelling electron microscopy (STEM) have been reported recently [13]. So far, defects in AlN samples were mainly studied under neutron irradiation, as discussed below. As to electron beam influence, this can result in both the excitation and ionization of AlN NT atoms [7]. In any case, a particle beam can be focused onto areas of several $Å^2$, which allows the selective modification of nanostructures on an atomic scale by removing atoms from pre-defined regions [11, 12]. The presence of intrinsic defects affects both the electronic and mechanical properties of NTs; they are also chemically active sites for nanotube wall functionalization. Despite noticeable interest to defective nanotubes, the number of publications about them is rather scarce, except for a series of studies on defective CNTs [11, 12, 14–17] and BN NTs [10, 18, 19]. The first paper, focused directly on the theoretical simulation of defective AlN SW NTs, was published only in 2006 [9], based mainly on DFT (density functional theory) plane-wave calculations of 1D SW NTs with different types of point defects or their pairs.

Beginning in the 1990s, electronic F centres (N vacancies) have been actively studied in AlN bulk [20–26], both experimentally and theoretically. According to a series of experimental studies [20], under thermal neutron irradiation of the wurtzite-structured AlN specimens, the appearance of F-type defects was indicated, with a strong correlation between the production of F centres and the intensity of neutron irradiation. The presence of the newly formed electronic F centres was identified using methods of electron paramagnetic or spin resonance (EPR or ESR), which show the appearance of spectral signals indicating an interaction between the electrons trapped at N vacancies and the surrounding Al nuclei. Optical transitions in defective AlN bulk are, in general, dominated by a broad luminescence band, which was attributed to a variety

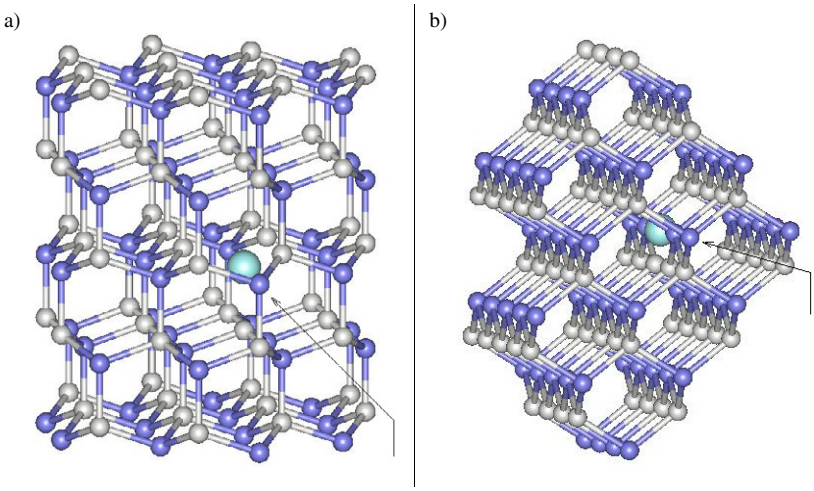

Figure 1. Axonometric images of supercells for the two AlN bulk phases containing single F centres: (a) wurtzite ($P6_3mc$ space group) and (b) zinc-blende ($F\bar{4}3m$ space group). Light balls correspond to Al atoms and N atoms are shown as dark balls whereas large balls image F centres. Arrows show directions of section planes used for construction of 2D difference electron density re-distributions induced by N vacancies, as presented in figure 4.

of point defects (e.g. N vacancies). It has been reported [22, 23] that each nitrogen vacancy induces two defect states in the band gap: one doubly occupied state lying above the top valence band (VB) and a higher-lying level structure that could be occupied with one or three electrons. For a stable AlN wurtzite-like structure (w-AlN), the upper defect state was found to be about 1–3 eV below the conduction-band (CB) minimum, i.e. the vacancy acts as a deep donor. For a metastable zinc-blende structure (zb-AlN), the same defect level, being much closer to the CB, can be considered as a shallow donor. In both cases, defects can affect both top VB and bottom CB, especially if their concentration is substantial. Defective AlN bulk 3D structures were calculated in the framework of several DFT plane-wave methods [21–25] or the embedded cluster HF (Hartree–Fock) method combined with a shell-model simulation [26]. Obviously, the results of these studies provide a foundation for the present theoretical simulations on the electronic structure of F centres in AlN NTs.

For this purpose, we perform DFT calculations in the framework of the CO LCAO formalism (crystalline orbitals constructed as linear combinations of atomic orbitals) on the structural and electronic properties of single F centres in: (i) defective AlN bulk (3D structures of both wurtzite an zinc-blende) (figure 1); (ii) defective AlN nanosheets which can be wrapped up into the corresponding 1 nm-thick AlN 1D SW NTs of armchair- and zigzag-type chiralities (figure 2); and (iii) defective 1 nm-thick AlN SW NTs of both chiralities (figure 3). In this study, we also analyse the influence of N vacancies on the properties of defective AlN SW NTs compared to those that we have obtained for defectless AlN nanotubes [8], depending on their chirality, and to those calculated for defective AlN bulk (both structural types). To achieve a dilute-limit single vacancy for both nanotube chiralities (figures 3(a) and (b)), we consequently increased the inter-defect distances along the NTs axes. For AlN bulk (figure 1), we consider large enough inter-defect distances, in order to exclude the appearance of noticeable dispersion of defect levels in the band gap. We also analyse the influence of F centres in AlN nanosheets (figure 2) on the energy required for wrapping up into AlN NTs. The results of our calculations

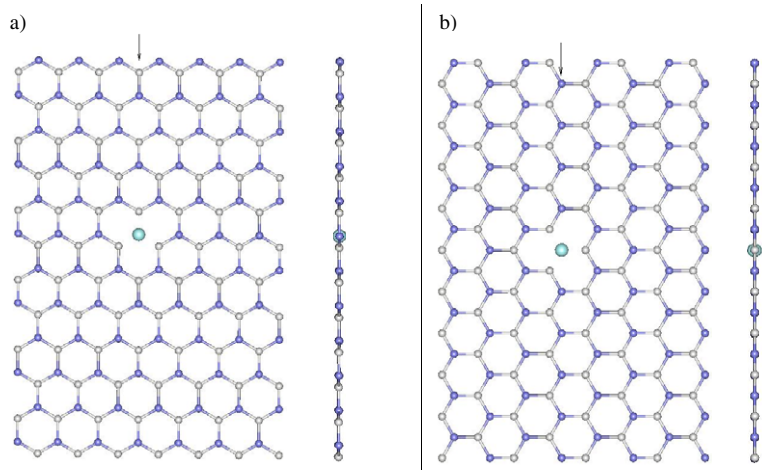

Figure 2. Projections of AlN nanosheets containing a single F centre for wrapping up to 1 nm-thick nanotubes (shown in figure 3) along the axes of NSs and across them for: (a) armchair-type and (b) zigzag-type chiralities. Arrows show section planes for 2D difference electron density plots presented in figure 6. For graphical details, see explanations given in figure 1.

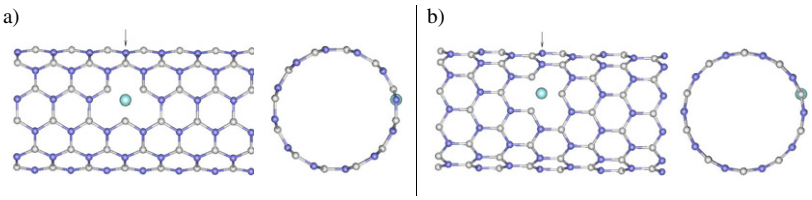

Figure 3. Projections of 1 nm-thick defective AlN NTs along the axes of nanotubes and across them for: (a) armchair-type and (b) zigzag-type chiralities. Arrows show section planes for 2D difference electron density plots shown in figure 8. For graphical details, see explanations given in figure 1.

are compared for the first time with a theoretical prediction of the electrical breakdown voltage reduction induced on defective AlN NTs upon the removal of a single Al–N bond.

2. Theoretical background

2.1. Computational details

We have performed periodic DFT calculations on the two models of defective AlN bulk (figure 1), two models of defective AlN (0001) nanosheets (figure 2) and two models of defective single-walled AlN nanotubes (figure 3) using the LCAO formalism of localized Gaussian-type functions (GTFs) as implemented in the *CRYSTAL-03* code [27]. For DFT calculations, we use the non-local PWGGA (Perdew–Wang generalized gradient approximation) exchange–correlation functional [28]. The all-valence basis sets for Al and N GTFs (8s–511sp–1d and 81s–31p–1d, respectively) were optimized elsewhere (for several Al-containing crystalline compounds [29] and gallium nitride [30]), we have only slightly re-optimized their valence and virtual shells. The F centres have been simulated by removing N atoms from all models considered (figures 1–3), retaining in the vacancy the wavefunction of the missing ion (the so-called *ghost* basis set [27]).

2.2. Supercell model of a periodic defective system

Use of a supercell model for point defect simulation means, in fact, consideration of a 'new periodic system' with an artificially introduced periodicity. The periodicity of the point defect is defined by the choice of supercell lattice, with the space group of the defective crystal defined by the defect local point symmetry [31]. The new Brillouin zone (BZ) is smaller than the primitive one and may also differ in symmetry, when the lattice type is changed. The calculation is otherwise made analogously to a perfect periodic system [8] using the k sampling of the BZ. For a fixed supercell size and shape, the k-meshes are used in practical calculations, which allow minimization of the defect–defect interaction. Use of variable k-meshes in a supercell model allows an estimate of defect–defect interaction through the width of the defect energy bands for each superlattice chosen (energy dispersion): the narrower these bands are (the smaller the dispersion), the closer the result to the single defect limit [31]. To achieve an approach of *single defect*, it is reasonable to begin from a smaller supercell containing an F centre, i.e. corresponding to the converged results of the band calculations. When estimating the defect–defect interaction from the calculated defect bandwidth, we make a decision about the necessity of a further increase in the supercell size. The comparison of results for different k-meshes allows one to decide if it is necessary to increase the superlattice further, to supresss artificial defect–defect interaction.

In this study, we simulate F centres in two AlN bulk phases using supercells with different defect periodicity: $3\times3\times3$ for wurtzite (figure 1(a)) and $4\times4\times4$ for zinc-blende (figure 1(b)). These extensions are chosen due to the close number of atoms in the corresponding w- and zb-AlN supercells (108 and 128, respectively, whereas a $3\times3\times3$ zb-AlN supercell contains 54 atoms only). Lattice parameters of both wurtzite and zinc-blende bulk structures have been optimized by us elsewhere [8]. A $3\times3\times3$ supercell corresponds to a inter-defect distance of $d_{\mathrm{F-F}} = 9.34$ Å, whereas for the $4\times4\times4$ supercell this distance is 12.45 Å. To simulate structural reconstruction around the point defect, we optimize geometry using the corresponding procedure of the *CRYSTAL-03* code [27].

When simulating defectless AlN graphitic nanosheets (NSs) shown in figure 2, but without F centres, we fix their lattice structures according to those for the unwrapped 1 nm-thick AlN NTs, geometries of which have been optimized in our previous paper (Al–N bond length $d_{\mathrm{Al-N}} = 1.79$ Å for both chiralities) [8]. Symmetry of both NSs is broken compared to the symmetry of armchair and zigzag-type NTs. However, each supercell of the corresponding AlN NS and NT contains the same number of atoms, and the strain energy required to wrap up an AlN graphitic nanosheet into the corresponding 1 nm single-walled nanotube can be defined simply as the difference between their total energies per atom. To avoid boundary artifacts, we periodically repeat NSs perpendicularly to their axes. When optimizing the NS geometry we allow the N sublattice to relax perpendicularly to the nanosheet plane, as in the 2D AlN(0001) surface. Al and N subplanes of perfect nanosheets of both chiralities were found to be separated by 0.016 Å, with almost negligible induced charges and dipole moments. For defective AlN nanosheets, we use the geometry of perfect NSs; however, atoms nearest to the single F centre are relaxed. We calculate the supercells of both defective AlN nanosheets (figures 2(a) and (b)) according to the inter-defect distances considered below for AlN NTs.

The symmetry of defective 1 nm-thick armchair- and zigzag-type AlN SW NTs is also broken compared to the corresponding defectless nanotubes studied by us previously [8] (Pn/m and $Pnmm$, respectively). For the defective armchair-type nanotube, only C_h symmetry of the cross-section plane remains (figure 3(a)), whereas for zigzag-type NT, no symmetry operations exist at all. Thus, calculations on defective AlN structures with relaxation of geometry around F centres performed in this study are much more space- and time-

consuming compared to our study of perfect AlN systems [8]. To approach a single vacancy limit for both nanotube chiralities, we have considered three sets of inter-defect distances repeated along the axes of these nanotubes: 13.5, 20.25 and 27.0 Å for armchair-type NT as well as 10.8, 21.6 and 32.4 Å for zigzag-type chirality.

The formation energies of a single F centre in all defective AlN systems presented in figures 1–3 are estimated as follows:

$$E^{\text{form}}(\text{F}) = E(\text{F}) + E(\text{N}) - E(\text{perfect system}), \tag{1}$$

where $E(\text{N})$ is the total energy for a spin-polarized isolated nitrogen atom (^{5}P state) per supercell, and $E(\text{F})$ and $E(\text{perfect system})$ are the corresponding energies for the defective and perfect periodic systems, respectively.

For the band structure calculations on all systems under study presented in figures 1–3, we use reciprocal space integration with suitable shrinking factors for the Monkhorst–Pack and Gilat nets: $4 \times 4 \times 8$ [32, 33]. The electron populations of atoms and inter-atomic bonds are estimated using a Mulliken approach, as implemented in *CRYSTAL-03* [27]. In section 3, we compare the structural and electronic properties calculated for all three types of defective systems: AlN bulk, NS and NT.

2.3. Charge concentration and electrical breakdown of defective nanotubes

Let us change the point of view and now consider an AlN SW NT or NS subjected to a given difference in voltage, generating a given current per bond i. If an elliptical hole of axes a and b (perpendicular and parallel to the electrical field, respectively) is introduced, the current will concentrate near the tip of the defect (which we assume to be much smaller than the structural size, i.e. we neglect the self-interaction of the tips or the defect–boundary interaction). Obviously, both models of defective NTs described here and in section 2.2 are different; however, we can compare charge concentrations induced on them.

Solving the Laplace equation for the corresponding perforated plate (two-dimensional continuum containing an elliptical hole) gives the spatial dependence of the current density [34]. By integration along the 'atomic spacing' q we find an approximate solution (asymptotic matching) for the tip charge concentration in a discrete lattice in the following form:

$$\frac{i_{\text{tip}}(a,b)}{i} \approx \sqrt{\frac{1+a/q}{1+a/q\,(1+a/b)^{-2}}}. \tag{2}$$

The approximation of the continuum (valid for a large defect with respect to the atomic size) would simply lead to $j_{\text{tip}}/j \approx 1 + a/b$ [34] with current density j, as can be deduced from equation (2) in the limit of $q \to 0$ (and formally $j = i/q$). The predictions of equation (2) are reported in table 1 as a function of the defect size and shape.

Accordingly, the electrical breakdown voltage of the defective system will be:

$$\frac{V_{\text{break}}(a,b)}{V_{\text{break}}^{(\text{defect-free})}} = \frac{i}{i_{\text{tip}}(a,b)}. \tag{3}$$

Thus, just a single vacancy can dramatically reduce the nanotube breakdown voltage, as has been similarly found for its fracture strength [35, 36] and (more moderately) for its Young's modulus [37].

3. Results and discussion

In our previous paper, we described the results of *ab initio* simulations on the structural and electronic properties for different morphologies of defectless AlN bulk, surfaces and

Table 1. Charge concentration (i_{tip}/i) as a function of the defect size and shape (a, b, q).

i_{tip}/i according to equation (2)											
	b/q										
a/q	0	1	2	3	4	5	6	7	8	9	10
0	1.00	1.00	1.00	1.00	1.00	1.00	1.00	1.00	1.00	1.00	1.00
1	1.41	1.26	1.18	1.13	1.10	1.09	1.07	1.06	1.06	1.05	1.05
2	1.73	1.57	1.41	1.32	1.26	1.22	1.19	1.17	1.15	1.13	1.12
3	2.00	1.84	1.64	1.51	1.42	1.36	1.31	1.27	1.24	1.22	1.20
4	2.24	2.08	1.86	1.70	1.58	1.50	1.43	1.38	1.34	1.31	1.28
5	2.45	2.30	2.06	1.88	1.74	1.63	1.55	1.49	1.44	1.40	1.36
6	2.65	2.50	2.26	2.05	1.89	1.77	1.67	1.60	1.54	1.49	1.45
7	2.83	2.69	2.44	2.22	2.04	1.90	1.79	1.71	1.64	1.58	1.53
8	3.00	2.86	2.61	2.38	2.18	2.03	1.91	1.81	1.73	1.67	1.61
9	3.16	3.03	2.78	2.53	2.32	2.16	2.02	1.92	1.83	1.75	1.69
10	3.32	3.19	2.93	2.68	2.46	2.28	2.14	2.02	1.92	1.84	1.77

nanotubes [8], comparing them with the available experimental and theoretical data. For the present DFT calculations on the defective AlN structures, we fix structural parameters optimized in that study (see table 1 and comments about it in [8]) and allow relaxation of only three coordination atomic spheres (circles) around the N vacancy. We perform calculations of w- and zb-AlN crystals containing single F centres not only for comparison of their properties with those for defective low-dimensional AlN systems (although it is also interesting, due to the difference in atomic coordination around point defects) but also for verification of the present computational scheme for an adequate description of defective AlN bulk structures. This exhaustive approach permits verification by comparison with materials studied quite comprehensively during the last 15 years.

3.1. F centres in AlN bulk

Relaxation of atoms nearest to a single F centre shows that the four nearest Al neighbours of the vacancy in both the w- and zb-AlN crystals are shifted by 0.10–0.11 Å from their lattice sites towards the defect, whereas the 12 next-nearest N atoms are also relaxed inwards but noticeably more weakly (0.03–0.04 Å) (table 2). The electronic charge induced on the F centre is -1.7 to $1.65e$ for non-relaxed w- and zb-AlN bulk. After relaxation of the nearest atoms the corresponding values are found to be slightly increased from -1.82 to $1.78e$, which can be explained by a closer approach between the vacancy and the Al neighbours. Since, in defect-free w- and zb-AlN bulk Mulliken analysis, the electronic charge on each N atom was found to be $-2.27e$ and $-2.22e$, respectively, the nearest neighbours of the vacancy additionally lose about $0.15e$ per Al compared to the same atoms in defect-free bulk. In all cases, the charge separation in w-AlN is a little bit larger compared to zb-AlN, including the electronic charge induced on the F centre. This is well illustrated by the difference in electron density plots in figure 4. The high intensity of the charge re-distribution in the area around the F centre is dominated by the electron density of broken Al–N bonds.

When comparing figures 4(a) and (b), which describe point defects distributed with various periodicities (9.34 and 12.45 Å, respectively), we can clearly observe a larger disturbance of the difference electron density in the first case. Obviously, even a $4 \times 4 \times 4$ supercell is not enough to exclude the defect–defect interaction and both band structures presented in figure 5 clearly demonstrate this, since defect levels are still not straight lines, i.e. their dispersions are

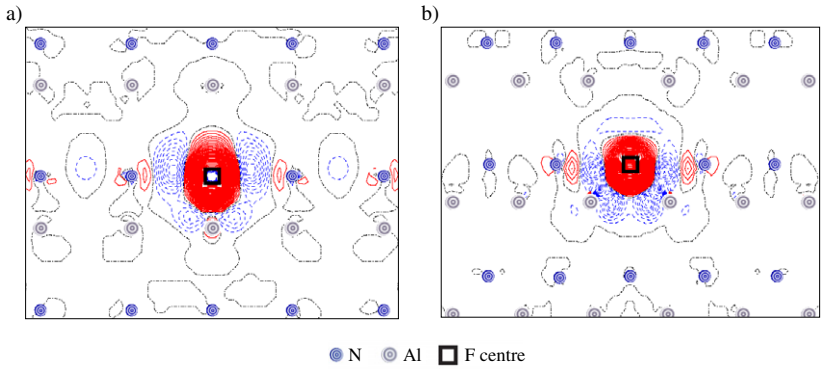

Figure 4. 2D difference electron density maps $\Delta\rho(\mathbf{r})$ (the *total density* in the perfect AlN bulk *minus the sum* of electron densities of both *isolated nitrogen atom* and *defective* AlN crystal) projected onto the (100) section plane of either (a) w-AlN (figure 1(a)) with one F centre per $3\times3\times3$ supercell or (b) zb-AlN (figure 1(b)) containing a single defect per $4\times4\times4$ supercell. Dash–dot *(black online)* isolines correspond to the zero level. Solid (*red*) and dashed (*blue*) isolines describe positive and negative values of the difference in electron density, respectively. Isodensity curves are drawn from -0.1 to $+0.1$ e Å^{-3} with increments of 0.003 e Å^{-3}.

Table 2. Main structural and electronic properties calculated for defective AlN bulk, SW NS and NT after partial geometry relaxation around F centre.

	Bulk (figure 1)		Nanosheets (figure 2)		Nanotubes (figure 3)	
Properties	w-AlN	zb-AlN	Armchair	Zigzag	Armchair	Zigzag
First sphere relaxation[a] $d_{\mathrm{F-Al}}$, (Å)	−0.10	−0.11	−0.17	−0.18	−0.22	−0.23
Second sphere relaxation[a] $d_{\mathrm{F-N}}$, (Å)	−0.03	−0.03	−0.05	−0.05	−0.07	−0.07
Charge induced on F centre Δq_F, (e)	−1.82	−1.78	−1.86[b]	−1.88[b]	−1.97[b]	−1.98[b]
Defect formation energy $E^{\mathrm{form}}(F)$, (eV)	8.8	8.6	7.7[b]	7.6[b]	7.2[b]	7.1[b]
Largest defect gap (versus band gap), $\Delta\varepsilon_{\max}$, (eV)	3.1 (7.4)	3.2 (7.2)	1.2 (2.5[c])	1.3 (2.5[c])	2.8 (7.1)	2.0 (7.0)

[a] Negative sign corresponds to inwards relaxation (towards F centre).
[b] These values are estimated for the largest inter-defect distances in NSs and NTs.
[c] We consider here a band gap for defectless w-AlN(0001) slab [8].

0.18 and 0.08 eV for w- and zb-AlN, respectively. As a further example, for a defective $SrTiO_3$ perovskite crystal [31], we identified a limit of single-defect approximation for inter-defect distances of 15–16 Å with dispersion of the defect level of ∼0.02 eV.

To estimate the formation energy of F centres in both w- and zb-AlN crystals (table 1) we use equation (1). Since it does not contain the chemical potentials of constituents [9, 22–25] we do not operate with Al-rich and N-rich defective structures and can verify our results only qualitatively. For non-relaxed w- and *zb*-defect-containing AlN bulk, E^{form} is found to be 9.9 and 9.5 eV, respectively (obviously, the formation energy for a lower concentration of point

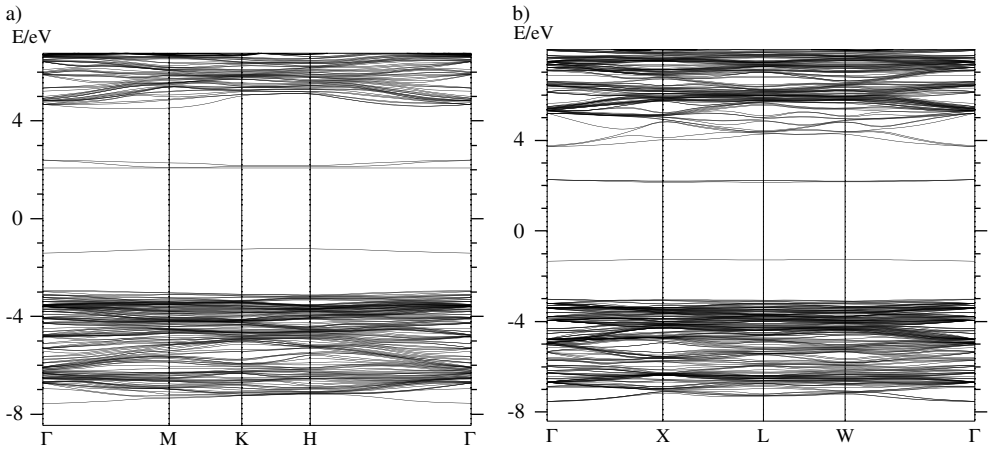

Figure 5. Two band structures of defective AlN bulk containing a single F centre per cell in both a $3 \times 3 \times 3$ supercell of a wurtzite crystal (a) and a $4 \times 4 \times 4$ supercell of a zinc-blende lattice (b).

defects should be lower), meanwhile the binding energy of Al–N bonds in defect-free w-AlN was also found to be larger by 0.12 eV than that in zb-AlN [8], i.e. the latter cubic structure is energetically less stable than wurtzite, which is well known. For defective AlN bulk structures relaxed around F centres, the values of the formation energies predictably decrease: 8.6 and 8.8 eV, for zb-AlN and w-AlN, respectively. For comparison, DFT plane-wave calculations of energies of N vacancy formation gave lower values: 6.6 eV [22] and 6.75 eV [25]. The reason for this 2 eV difference is due not only to certain differences in binding energy definitions. According to our experience, application of the DFT plane-wave method results in smaller values of E^{form} than given by the compatible DFT-LCAO method with the same exchange-correlation functional [31] (in both cases we use equation (1) to estimate the formation energy).

Our previous band structure calculations for defect-free AlN bulk resulted in values of 7.4 and 7.2 eV for the band gaps of w- and zb-AlN, respectively (cf 6.28 eV obtained experimentally for the stable wurtzite phase) [8]. The corresponding values obtained using plane-wave DFT calculations were found to be in an interval of 4.8–5.7 eV [21–25]. We again face some systematic gap between the estimated energies calculated using different methods. According to earlier DFT plane-wave calculations [22, 23] of the defective AlN band structure, there are two defect levels induced by the N vacancy to be moved into the band gap: (i) the a_1 (Al s-like) state lies 0.5–1.5 eV above the top valence band (VB); (ii) the t_2 (Al p-like) state is positioned below the bottom of the conduction band (CB) for w-Al and much closer to it or even higher for zb-Al. Our results presented in figure 5 and table 2 give 1.5–1.8 eV over the top VB for the a_1 state and 1.7–2.2 eV below the CB bottom for the t_2 state, which is twice degenerate for both phases. In any case, the calculated defect levels can be verified experimentally by luminescence measurements [4]. We have identified a problem for plane-wave DFT calculations that, due to an underestimated band gap, the shallow defect states, which should be positioned below the CB, are found sometimes at the level of its bottom and even higher [38]. This problem may likely be solved after the implementation of hybrid HF-DFT functionals in the computational procedure of plane-wave calculations [39], which allows one to achieve values of band gaps that are quantitatively compatible with experimental data. Note that we do not consider the charged N vacancies, the presence of which substantially complicates the composition of defect levels. Such analysis was performed

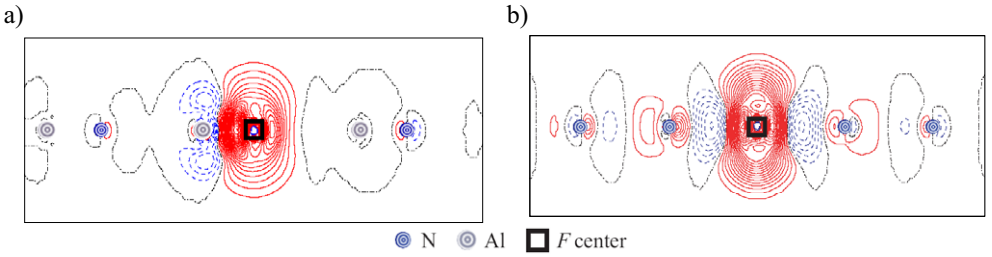

Figure 6. 2D difference electron density maps $\Delta\rho(\mathbf{r})$ (see explanations given in figure 4) projected onto the section planes across AlN NS containing a single F centre per doubly extended unit cell with a structure of (a) armchair-type (figure 2(a)) or (b) zigzag-type (figure 2(b)) NS chiralities. For graphical details, see explanations given in figure 4.

in several studies [23, 24, 26] where the charge of the nitrogen vacancy was changed from +1 up to +3. For the composition of charged vacancies, resonance defect states can be positioned at the CB bottom.

3.2. F centres on SW AlN nanosheets

Two types of graphitic nanosheets (figure 2) with slightly separated Al and N sublattices can be considered as orthogonal nanofragments of a 2D double-layer AlN(0001) surface (planar sheet). It should be noticed that a graphitic sheet is a stable phase of carbon and boron nitride materials [40, 41], whereas AlN materials with the same configuration have not been synthesized experimently so far. This is probably due to the highest strain energy of AlN graphitic sheet relative to w-AlN and zb-AlN structures compared to other group-III nitrides [5, 40]. Moreover, the experimental growth of NT structures is thought to have little to do with rolling up graphitic nanosheets. Nevertheless, AlN NSs are interesting from several points of view: (i) the strain energies in NTs relative to their graphitic NS materials are always regarded as important references in analysing the probability of nanotubular synthesis [42]; (ii) the electronic structure of nanosheets reflects some specific AlN surface properties which markedly differ from those for bulk and nanotubes [8]; (iii) difference between single F centres in both NSs and NTs allows one to understand better the structural transformations in nanomaterials.

In AlN nanosheets, nanotubes as well as the surface layer coordination of Al and N atoms as well as F centres are reduced compared to that in the bulk: each of them possesses three nearest neighbours instead of four. Compared to atomic relaxation around a single F centre in AlN bulk, these three nearest Al neighbours of the F centre in the AlN NS relax more strongly, i.e. by 0.17–0.18 Å towards the point defect, the six next-nearest N atoms (instead of 12 in the bulk) are also shifted inwards more noticeably than in the bulk (table 2). Qualitatively, this is quite understandable, since low-dimensional systems are usually more flexible for atom relaxation. For the non-relaxed armchair- and zigzag-type AlN NS, the electronic charge induced on the F centre is smaller than in the bulk (-1.57–$1.59e$); however, after relaxation the corresponding values increase more substantially than in the bulk (-1.86–$1.88e$ versus -1.78–$1.82e$). The 2D charge re-distributions induced by the F centre in both NSs (figure 2) are shown in figure 6.

The formation energies of a single F centre onto *non-relaxed* armchair- and zigzag AlN nanosheets are found to be 8.6 and 8.4 eV, respectively (table 2), i.e. quite predictably smaller than those in AlN bulk. For defective AlN nanosheet structures *relaxed* around F centres,

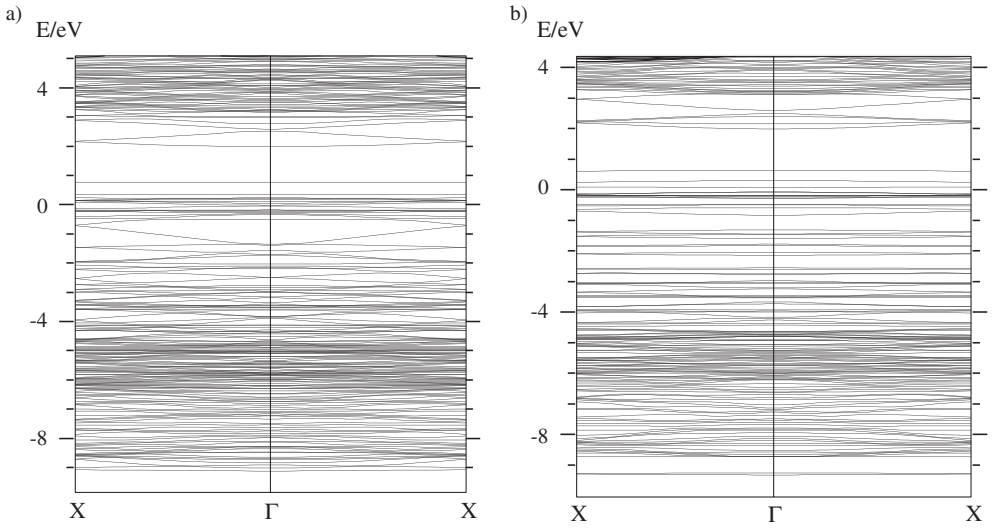

Figure 7. Two band structures of defective AlN nanosheets containing a single F centre per doubly extended unit cell of armchair-type (a) and zigzag-type (b) NS chiralities.

the corresponding values of formation energies decrease to 7.7 and 7.6 eV for armchair- and zigzag-type chiralities, respectively. For comparison, the energy of N vacancy formation on a planar hexagonal BN sheet was earlier found to be 8.9 eV [10]. (Note that, when comparing the energies of F centre formation in BN and AlN bulk [22], E^{form} was found to be larger by 1.5–2 eV for the former.)

Our previous band structure calculations on defect-free densely packed w-AlN(0001) and zb-AlN(111) surfaces published elsewhere [8] showed the appearance of spectra of the surface states inside the band gap, consisting of hybridized Al(3s), Al(3p) and N(2p) energy levels (note that the top VB of AlN surfaces is shifted up by ∼3 eV compared to the AlN bulk). Analogous conclusions were earlier drawn for the densely packed w-GaN(0001) surface [43] as well as less dense w-AlN($10\bar{1}0$) and zb-AlN(110) surfaces [44]. This provides a reason for the marked difference between the band structures presented in figures 5 and 7. In the latter, we can identify two groups of degenerate defect levels induced by an N vacancy in the band structure of defective AlN NSs: Al(3s) states lying ∼0.7–0.8 eV above the top VB and Al(3p) states which are positioned below the CB bottom by ∼1.0–1.1 eV.

Let us estimate the strain energies required to wrap up AlN graphitic SW nanosheets (figure 2) into the corresponding 1 nm SW nanotubes (figure 3). The corresponding results for energy cost per atom are found to be 0.078 eV/atom (armchair chirality) and 0.091 eV/atom (zigzag chirality), which is in good quantitative agreement with previously calculated values for SW NTs with the same 1 nm diameter (0.05 and 0.06 eV/atom, respectively [38]). Analogous transformation from nanosheets to nanotubes containing F centres requires slightly smaller energy cost (by 0.008 eV/atom for both chiralities), i.e. the presence of point defects makes wrapping up an NS into an NT easy. Comparative analysis performed earlier [38] shows that the energy cost of forming AlN SW NT from graphitic nanosheets is the lowest compared to other group-III nitrides and carbon. At the same time, the AlN graphitic sheet is the most unstable energetically among these nanosheets. It should also be noticed that the larger the single-walled nanotube diameter is, the smaller this energy barrier NS → NT [5, 40] is, i.e. a nanotube of infinite diameter becomes a graphitic plane or (0001) bilayer surface. This confirms

a conclusion made in our previous paper [8]: the larger the AlN SW NT diameter is, the closer the nanotube's electronic properties are to double-layer surface properties; analogous results were earlier obtained for GaN NTs [42]. On the other hand, the excessively high strain energy of an AlN graphitic sheet relative to the stable w-AlN bulk structure, as a main reason of instability for both AlN SW NSs and NTs, can be reduced by the consequent growth of the nanotube wall thickness through a nanorod to a nanowire, the internal structure of which is close to wurtzite and the cross section of which is similar to a quasi-hexagon [5]. For this type of nanomaterial, the larger the diameter is, the closer its properties are to the bulk. However, the reproducible synthesis of quasi-cylindrical AlN SW NTs and coaxially-cylindrical AlN MW NTs remain important practical goals, since similar configurations of CNTs and BN NTs possess numerous technological applications [10–12, 14–19].

3.3. F centres on SW AlN nanotubes

Atom relaxations around a single F centre for both chiralities of AlN SW NTs (figure 3) are found to be larger than in AlN bulk and graphitic nanosheet (table 2): the three nearest Al neighbours of an N vacancy are shifted by 0.22–0.23 Å from their lattice sites towards the defect and inside the nanotube, whereas the next-nearest N atoms are relaxed in the same directions more weakly (0.07–0.08 Å). Note that the structural optimization around a single F centre for both armchair- and zigzag-type AlN nanotubes has been performed only for the smallest inter-defect distances considered in this study (13.5 and 10.8 Å, respectively), Then, due to the limited possibility of the *CRYSTAL-2003* code [27] for geometry optimization of large systems (up to 240 atoms per supercell) with a minimal number of symmetry operators (as described in section 2.2), we have used these relaxed configurations around the corresponding F centres for defective AlN NTs with larger inter-defect distances. The electronic charges induced on point defects in the case of non-relaxed armchair- and zigzag-type AlN NTs are -1.75 and $-1.76e$, respectively, being markedly increased after relaxation, up to -2.06 and $-2.08e$ for the smallest inter-defect distances versus -1.97 and $-1.98e$ for the largest distances. Obviously, the latter may be considered as more reliable charges, where inter-defect interaction is practically absent. Charge re-distributions induced by the F centre in both nanotubes (figure 3) are shown in figure 8. Note that we increase the isoline density compared to figures 4 and 6, in order to illustrate better details of the electronic charge re-distributions around F centres. For the cross-section of an armchair-type AlN NT, one can observe a larger charge delocalization across the nanotube (figure 8(a)); however, for zigzag-type NTs, charge re-distribution is more delocalized along the nanotube.

The formation energies of a single F centre onto *non-relaxed* armchair- and zigzag-type AlN nanotubes are found to be 8.1 and 7.9 eV, respectively (table 2), i.e. considerably smaller than those in AlN nanosheets. For defective AlN nanotube structures *relaxed* around F centres, the corresponding values of formation energies decrease to 7.2 and 7.1 eV for armchair- and zigzag-type chiralities, respectively. For comparison, the energy of N vacancy formation on zigzag-type BN nanotubes of 1.25 nm-thick diameter was earlier found to be 8.2 eV [10]. (Note that, when comparing the energies of F centre formation in BN and AlN bulk [20], E^{form} was found to be larger by 1.5–2 eV for the former.)

Our previous band structure calculations on defect-free AlN nanotubes [8] gave band gaps of 7.1 and 7.0 eV for the armchair- and zigzag-type 1 nm-thick AlN NTs, respectively, which are confirmed by current calculations on defective NTs (figure 9). However, the corresponding nanotube values obtained using plane-wave DFT calculations were found to be in the interval 3.0–4.0 eV [5, 9, 40], i.e. again underestimated, analogously to those discussed for AlN bulk. We have calculated AlN NTs for three sets of inter-defect distances repeated along the axes

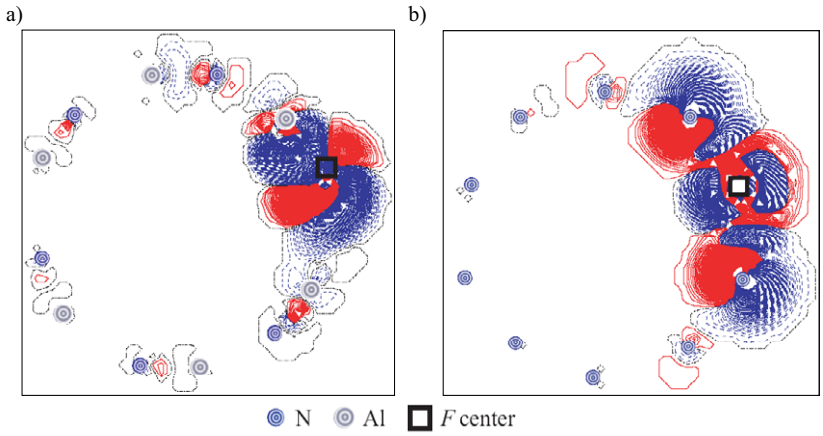

Figure 8. 2D difference electron density maps $\Delta\rho(\mathbf{r})$ (see explanations given in figure 4) projected onto the section planes across AlN NT containing a single F centre per doubly extended unit cell with a structure of (a) armchair-type (figure 3(a)) or (b) zigzag-type (figure 3(b)) NT chiralities. For graphical details, see explanations given in figure 4. To increase the resolution of both charge density plots, we have drawn isodensity curves from -0.3 to $+0.3$ e Å^{-3} with increments of 0.001 e Å^{-3}.

of both nanotubes. However, we present the band structures for the two sets for each type of NT (figures 9(a)–(d)) since, for the largest inter-defect distances (27.0 Å for an armchair-type NT as well as 32.4 Å for zigzag-type chirality), the band structure almost coincides with that for the middle inter-defect distance (20.25 Å or 21.5 Å, respectively); the only difference here is a higher band density in both VB and CB areas, whereas positions of defect levels in band gaps are practically identical. The interaction between the defects in this case is found to be negligible, since the energy dispersion of defect levels in both band structures (figures 9(c) and (d)) does not exceed 0.02 eV, thus these defect levels look like straight lines. This allows us to conclude that, for $d_{\mathrm{F-F}} \geqslant 20$ Å, the periodic F centre can be described as a single defect. Moreover, for these distances, we observe a similarity in band structures for both NT chiralities (figures 9(c) and (d)). The largest difference between the band structures of armchair- and zigzag-type NTs is observed for the smallest inter-defect distances (figures 9(a) and (b)). As for AlN bulk (figure 5), there are two defect levels induced by the N vacancy inside the NT band gap: (i) the a_1 energy level, consisting of mainly an Al(3s) state partially hybridized with Al(3p), which lies ∼3.1 and ∼2.8 eV above the top VB for armchair- and zigzag-type structure, respectively; (ii) the doubly degenerate t_2 energy level, consisting of mainly Al(3p) with a partial contribution from Al(3s), which is positioned either 2.3–2.4 eV below the bottom of the CB for armchair-type AlN NTs, with a small state splitting (∼0.1 eV), or 1.5 eV below the same bottom for zigzag-type AlN NTs (this is true for the highest defect level, since splitting here is substantial, ∼1.0 eV). In both band structures we observe a pair of levels split off the top VB (figures 9(a) and (b)), which are both doubly degenerate in defective zigzag-type NT. Obviously, these are pure nanotube levels observed by us also in the corresponding DOSs of defect-free AlN nanotubes (figure 6 in [8]) which consist of Al(3s) and partially Al(3p) states. When comparing our results with the band structure of 1 nm-thick zigzag-type SW NT calculated by Simeoni etc [9], we can conclude that, due to underestimation of the band gap in that study, both a_1 and t_2 levels are too close to the CB bottom, although their position relative to the top VB is qualitatively close to our results (2.25 versus 2.8 eV). For zigzag-type AlN NT with small inter-defect distances (figure 9(b)) the largest inter-defect (or defect-VB&CB)

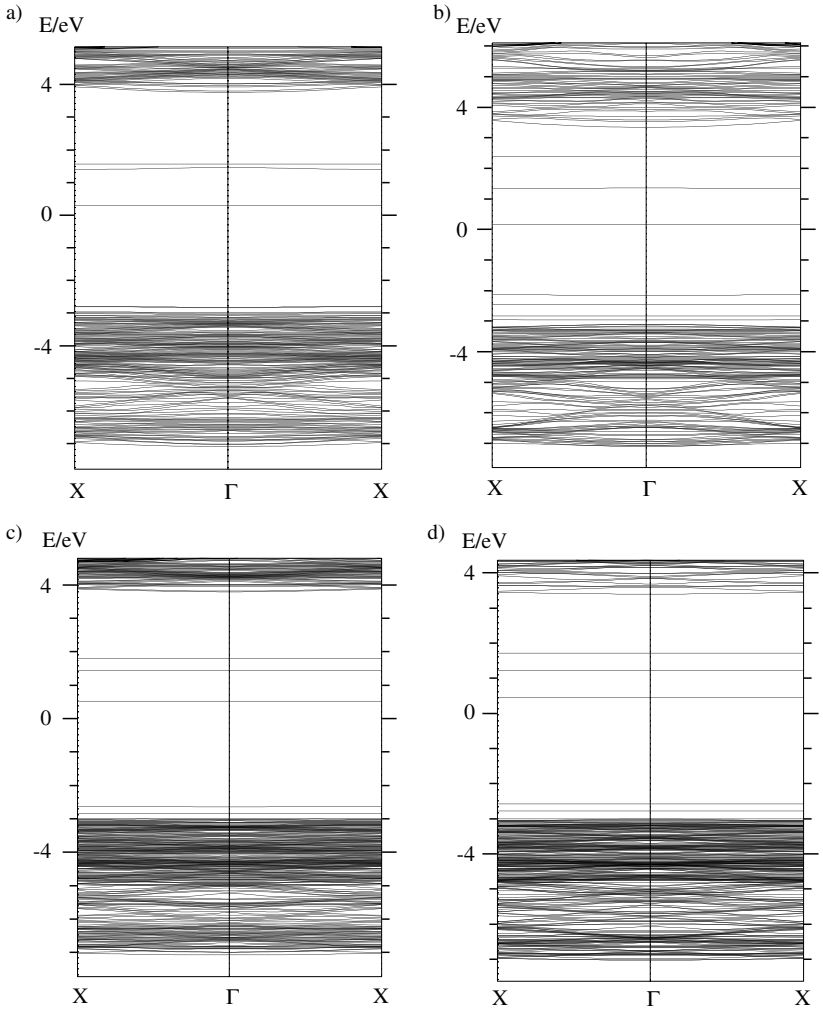

Figure 9. Four band structures of defective AlN nanotubes containing a single F centre on either armchair-type NT (for inter-defect distances (a) 13.5 Å and (c) 20.25 Å) or zigzag-type NT (with the corresponding distances (b) 10.8 Å and (d) 21.6 Å).

gap is found to be ∼2.2 eV (cf 7.0 eV for the whole band gap); for larger inter-defect distances this gap increases to 2.8 eV. This means that the higher the F centre concentration is in at least zigzag-type AlN NT, the closer its electronic properties is to an AlN graphitic sheet.

3.4. Comparative analysis of F centre properties in AlN bulk, graphitic sheets and nanotubes

Let us summarize in table 2 the main parameters calculated in the current study. We compare (i) relaxation of atoms around the F centre, $d_{F-\mathrm{Al}}$ and $d_{F-\mathrm{N}}$; (ii) the electronic charge induced on the F centre, Δq_{F}; (iii) the formation energy E^{form}; (iv) the largest energy gap between the defect (surface) levels and/or the top VB (bottom of the CB) $\Delta\varepsilon_{\mathrm{max}}$ (compared with the band gap for the perfect structure in brackets). The results obtained by us previously have been systematized elsewhere (table 1 in [8]).

Analysis of different values in table 2 as well as charge re-distributions in figures 4, 6 and 8 clearly demonstrates that the relaxation of atoms nearest to the N vacancy in AlN nanotubes is much stronger than that in AlN bulk (both phases) and even graphitic sheet. These results confirm conclusions drawn in recent studies of defective CNT [11, 12]: the main reason for the larger atomic relaxation in nanotubes is found to be the strained NT structure compared to the bulk and surface. Nevertheless, unlike CNT, the dangling bonds around the N vacancy in AlN nanotubes of both chiralities ended by Al atoms cannot create new covalent (or metallic) bonds in the vicinity of the F centre, since the periodic Madelung potential results in electrostatic stabilization of the electronic charges trapped in the vacancies [45].

At the same time, it is well known that F_s centres at ionic surfaces are chemically reactive towards both deposited metals (including Ag and Cu [46]) and gases (including chlorine [47]). Thus, theoretical simulation of F centre reactivity in AlN nanotubes is of great interest. Meanwhile, in a recent theoretical study of defective zigzag-type AlN NT, the dangling bond saturation around the N vacancy was already achieved by the Al_N antisite as well as C_N and O_N substitutes [9]. The Al atom as a substitute for N in the AlN NTs was found to hang out of the tube by 1.5 Å, thus indicating its relative instability compared to the substituted N atom. Moreover, an increase of Al local content in the vacancy area does not result in the occurrence of local metallic behaviour: two well-separated defect states with a Fermi level in the middle between them appear in the gap. Both C_N and O_N substitutes do not introduce strong lattice deformations, since they are structurally similar to the missing N atom. In the presence of O_N impurities in AlN NT, the Fermi level crosses a new band which arises in the gap, thus leading to partly metallic behaviour, but this defect also introduces two electronic states in the gap, which is more typical for defects in semiconductors [9]. On the other hand, a C_N defect simply introduces these electronic states into the band gap, similarly to an F centre; however, unlike the latter, the Fermi level for C_N substitute was found to be much closer to the top VB.

3.5. Prediction of quasi-continuum model for defect charge concentration

Using equation (2) for a single vacancy in AlN NT ($a = b = q$), we find $i_{\text{tip}}/i \approx \sqrt{8}/5 \approx 1.26$. This prediction can be verified according to the following procedure. If an AlN bond is removed from the nanotube, the current will concentrate in the bonds nearest to the missing one. Assuming linearity, the current around the missing bond (i_{tip}) is equal to the superposition of the currents in the defectless nanotube with the same external source (i) and generated in the system by a dipole voltage source placed along the missing bond (without the external source). This problem can be solved analytically for a two-dimensional square lattice [32], giving $i_{\text{tip}}/i \approx 4/\pi \approx 1.27$, which is close to our previous prediction. Our *ab initio* calculations show qualitatively similar charge redistributions due to single F centres (e.g. $2.27/1.75 = 1.29$ and $2.26/1.76 = 1.28$ for the non-relaxed armchair- and zigzag-type NTs, or $2.21/1.97 = 1.13$ and $2.20/1.98 = 1.11$ for the relaxed nanotubes, respectively), suggesting that quasi-continuum approaches can be applied qualitatively in the study of nanosystems. Despite the difference between both defective nanotube models, we can similarly describe the charges around defects in non-relaxed NTs.

4. Summary

In the present paper we have discussed the results of systematic non-local DFT (PWGGA) calculations on defective (N vacancy containing) single-walled 1 nm-thick AlN nanotubes possessing two different chiralities (armchair- and zigzag-type), single-walled nanosheets, which can be wrapped up into the corresponding AlN NTs, and two phases of AlN bulk. In

performing the calculations we analyse their structural and electronic properties, comparing them with available data in the literature. It should be underscored that the point defect and yet more complicated defects are certainly present in experimentally synthesized NTs, so their careful theoretical study is necessary for a reliable comparison with the corresponding experimental data. Our current calculations are performed for neutral defects, and therefore further studies are necessary to understand what happens for different charge states. We also ignored the magnetic properties of AlN materials, which can be important for a better understanding of defective nanostructures. In this study, we have focused on N vacancies (F centres) only, although the presence of Al vacancies, Al_N and N_{Al} antisite substitutes as well as C and O impurities, is well established in AlN nanomaterials [9] and their study is of great importance. Finally, we limit ourselves to the SW model of an AlN NT, although the majority of experimentally synthesized AlN nanotubes should be considered as MW NTs with either wurtzite or zinc-blende structure [5, 7].

Nevertheless, we believe that our results qualitatively describe certain aspects of real AlN nanomaterials, which can be verified experimentally, for instance by using various methods of luminescence and photoelectron spectroscopy. For this purpose, we predict several points; for instance, we established a separation limit for an isolated defect in AlN nanotubes (20 Å), and we show that the larger the content of N vacancies in NT is, the closer its electronic structure is to an AlN surface with substantially smaller band gap compared to the defectless bulk or nanotubes of small diameters. Our results summarized in table 2 also show that the zigzag-type chirality of AlN nanotubes is energetically more favourable and is probably prevalent in experimentally synthesized samples. Some results are quite interesting from the fundamental point of view, for example when we compare the properties of defective AlN bulk, graphitic sheets and nanotubes. We confirm a conclusion from our previous study [8] that the larger the diameter of an AlN SW NT is, the closer its properties are to an AlN thin film, which can be considered as a fragment of AlN NTs of infinite diameter. An additional advantage of the current study is that we compare results obtained using two different theoretical approaches; for example, the charge re-distributions around single defects in AlN NTs calculated using the DFT-LCAO method are qualitatively comparable to those predicted when applying the simplified quasi-continuum approach [32–34]. On the whole, we believe that the current study can be considered as one of initial steps to gain a deeper insight into the new, technologically important nanomaterials.

Acknowledgments

This study was supported by both the Latvian National Program on Nanomaterials and Nanotechnologies (no. 05.0026.1.1) as well as the Materials Research Science and Engineering Center (MRSEC) Program of the National Science Foundation (DMR-0520513) at the Materials Research Center of Northwestern University (NU), Evanston, USA. YZ kindly thanks D E Ellis, B Berzina and L Trinkler for fruitful discussions as well as members of the Materials Theory Group at NU for hospitality and good collaboration during his stay there. The technical assistance of S Piskunov was most valuable.

References

[1] Golberg D, Bando Y, Eremets M, Takemura K, Kurashima K and Yusa H 1996 *Appl. Phys. Lett.* **69** 2045
[2] Hu J, Odom T W and Lieber C M 1999 *Acc. Chem. Res.* **32** 435
[3] Bellucci S 2005 *Nucl. Instrum. Methods* B **234** 57
Bellucci S 2005 *Phys. Status Solidi* c **2** 34

[4] Shi S C, Chen C F, Chattapodhyay S, Chen K H, Ke B W, Chen L C, Trinkler L and Berzina B 2006 *Appl. Phys. Lett.* **89** 163127
[5] Zhao M, Xia Y, Liu X, Tan Z, Huang B, Song C and Mei L 2006 *J. Phys. Chem.* B **110** 8764
[6] Wu Q, Hu Z, Wang X, Lu Y, Chen X, Xu H and Chen Y 2003 *J. Am. Chem. Soc.* **125** 10176
[7] Balasubramanian C, Godbole V P, Rohatgi V K, Das A K and Bhoraskar S V 2004 *Nanotechnology* **15** 370
Balasubramanian C, Bellucci S, Castrucci P, De Crescenzi M and Bhoraskar S V 2004 *Chem. Phys. Lett.* **383** 188
Bellucci S 2004 *CANEUS 2004-Conf. on Micro-Nano-Technologies (Monterey, CA, USA, Nov. 2004)* AIAA paper 2004-6752
Balasubramanian C, Bellucci S, Cinque G, Marcelli A, Cestelli Guidi M, Piccinini M, Popov A, Soldatov A and Onorato P 2006 *J. Phys.: Condens. Matter* **18** S2095
Bellucci S, Balasubramanian C, Ivanov A, Popov A and Schober H 2006 *J. Neutron Research.* **14** 287
[8] Zhukovskii Yu F, Popov A I, Balasubramanian C and Bellucci S 2006 *J. Phys.: Condens. Matter* **18** S2045
[9] Simeoni M, Santucci S, Picozzi S and Delley B 2006 *Nanotechnology* **17** 3166
[10] Zobelli A, Ewels C P, Gloter A, Seifert G, Stephan O, Csillag S and Colliex C 2006 *Nano Lett.* **6** 1955
[11] Lu A J and Pan B C 2004 *Phys. Rev. Lett.* **92** 105504
[12] Sammalkorpi M, Krasheninnikov A, Kuronen A, Nordlund K and Kaski K 2004 *Phys. Rev.* B **70** 245416
Krasheninnikov A V, Banhart F, Li J X, Foster A S and Nieminen R M 2005 *Phys. Rev.* B **72** 125428
Krasheninnikov A V, Lehtinen P O, Foster A S and Nieminen R M 2006 *Chem. Phys. Lett.* **418** 132
[13] Mkhoyan K A, Batson P E, Cha J, Schaff W J and Silcox J 2006 *Science* **312** 1354
[14] Ajayan P M, Ravikumar V and Charlier J-C 1998 *Phys. Rev. Lett.* **81** 1437
[15] Ouyang M, Huang J-L and Lieber C M 2002 *Phys. Rev. Lett.* **88** 066804
[16] Sternberg M, Curtiss L A, Gruen D M, Kedziora G, Horner D A, Redfern P C and Zapol P 2006 *Phys. Rev. Lett.* **96** 075506
[17] Carlson J M 2006 *Phys. Status Solidi* b **243** 3452
[18] Schmidt T M, Baierle R J, Piquini P and Fazzio A 2003 *Phys. Rev.* B **67** 113407
Piquini P, Baierle R J, Schmidt T M and Fazzio A 2005 *Nanotechnology* **16** 827
[19] Miyamoto Y, Rubio A, Berber S, Yoon M and Tomanek D 2004 *Phys. Rev.* B **69** 1214013
[20] Honda M, Atobe K, Fukuoka N, Okada M and Nakagawa M 1990 *Japan. J. Appl. Phys.* **29** L652
Atobe K, Okada M and Nakagawa M 2000 *Nucl. Instrum. Methods Phys. Res.* B **166/167** 57
[21] Mattila T and Nieminen R M 1996 *Phys. Rev.* B **54** 16676
Mattila T and Nieminen R M 1997 *Phys. Rev.* B **55** 9571
[22] Gorczyca I, Christensen N E and Svane A 1997 *Solid State Commun.* **101** 747
Gorczyca I, Svane A and Christensen N E 1999 *Phys. Rev.* B **60** 8147
[23] Stampfl C and Van der Walle C G 1998 *Appl. Phys. Lett.* **72** 459
Stampfl C and Van der Walle C G 2002 *Phys. Rev.* B **65** 155212
[24] Fara A, Bernardini F and Fiorentini V 1999 *J. Appl. Phys.* **85** 2001
[25] Tanaka I, Tatsumi K, Nakano M and Adachi H 2002 *J. Am. Ceram. Soc.* **85** 68
[26] Vail J M, Schindel D, Yang A, Penner O, Pandey R, Jiang H, Blanco M A, Costales A, Qiu Q C and Xu Y 2004 *J. Phys.: Condens. Matter* **16** 3371
Vail J M, Chevrier D K, Pandey R and Blanco M A 2006 *J. Phys.: Condens. Matter* **18** 2125
[27] Saunders V R, Dovesi R, Roetti C, Orlando R, Zicovich-Wilson C M, Harrison N M, Doll K, Civalleri B, Bush I J, D'Arco Ph and Llunell M 2003 *CRYSTAL-03 User Manual* University of Turin
[28] Perdew J P and Wang Y 1986 *Phys. Rev.* B **33** 8800
Perdew J P and Wang Y 1989 *Phys. Rev.* B **40** 3399
Perdew J P and Wang Y 1992 *Phys. Rev.* B **45** 13244
[29] Catti M, Valerio G, Dovesi R and Causá M 1994 *Phys. Rev.* B **49** 14179
[30] Gulans A, Evarestov R A, Tale I and Yang C C 2005 *Phys. Status Solidi* c **2** 507
[31] Evarestov R A, Kotomin E A and Zhukovskii Yu F 2006 *Int. J. Quantum Chem.* **106** 2173
[32] Monkhorst H J and Pack J D 1976 *Phys. Rev.* B **13** 5188
[33] Gilat G 1982 *Phys. Rev.* B **26** 2243
[34] Duxbury P M, Leath P L and Beale P D 1987 *Phys. Rev.* B **36** 367
[35] Pugno N M and Ruoff R S 2004 *Phil. Mag.* **84** 2829
[36] Pugno N M 2006 *Int. J. Fract.* **140** 159
Pugno N M 2006 *Int. J Fract.* **141** 313
Pugno N M 2006 *J. Phys.: Condens. Matter* **18** S1971
[37] Pugno N M 2007 *Appl. Phys. Lett.* **90** 043106
[38] Zhukovskii Yu F, Evarestov R A, Kotomin E A, Mastrikov Yu A, Piskunov S N and Shunin Yu N 2006 *Comput. Model. New Technol.* **10** 14

[39] Paier J, Hirschl R, Marsman M and Kresse G 2005 *J. Chem. Phys.* **122** 234102
[40] Zhao M, Xia Y, Tan Z, Liu X, Li F, Huang B, Ji Y and Mei L 2004 *Chem. Phys. Lett.* **389** 160
[41] Orellana W and Chacham H 2001 *Phys. Rev.* B **63** 125205
[42] Lee S M, Lee Y H, Hwang Y G, Elsner J, Porezag D and Frauenheim Th 1999 *Phys. Rev.* B **60** 7788
[43] Zywietz T K, Neugebauer J and Scheffler M 1999 *Appl. Phys. Lett.* **74** 1695
[44] Pandey R, Zapol P and Causá M 1997 *Phys. Rev.* B **55** 16009
[45] Ferrari A M and Pacchioni G 1995 *J. Phys. Chem.* **99** 17010
[46] Fuks D, Zhukovskii Yu F, Kotomin E A and Ellis D E 2006 *Surf. Sci.* **600** L99
[47] Xu Y J, Li J Q, Zhang Y F and Chen W K 2004 *J. Chem. Phys.* **120** 8753